JOURNAL OF MATERIALS SCIENCE 20 (1985) 3339 – 3352

A comparison of the structural evolution occurring during anisothermal or isothermal treatments in the case of nickel and manganese type maraging alloys

J. B. LECOMTE*, C. SERVANT*, G. CIZERON‡
Laboratoire de Métallurgie Physique, Bât. 413, and ‡Laboratoire de Structure des Matériaux Métalliques, Bât. 465, Université Paris Sud, Centre d'Orsay, 91405 Orsay Cedex, France

This paper reports a comparison of the structural evolution of nickel and manganese type maraging steels. The dilatometric behaviour was studied during anisothermal treatments performed at different rates. Furthermore, the evolution of the microstructure was followed during isothermal ageing with the help of electron microscopy and microdiffraction.

1. Introduction

Vascomax 300 grade maraging steels having a composition of 18.5 Ni–8.9 Co–4.8 Mo–0.6 Ti–0.1 Al–0.05 Cu–Fe balance (wt %) have been first developed by Decker and co-workers since 1962 [1, 2], and later on were studied with regard to either structural transformations or their mechanical properties [3–13]. In order to identify the influence of the different addition elements nickel, cobalt and molybdenum on the two precedent points, simplified steels of Fe–Ni–Co, Fe–Ni–Mo and Fe–Ni–Co–Mo types were prepared. Taking into account the cost price of manganese as compared to that of nickel, it was interesting to study the influence of substituting manganese by nickel in these synthesized alloys or steels. In the literature, there exist only a few works relative to manganese alloys with a composition near that of maraging steels [14–17].

2. Experimental procedure

The alloys were prepared from the mixtures of high-purity powders (the characteristics of which are given in Table I) by solid-state sintering processing. The green pellets were compressed under a pressure of 500 MPa and then sintered at 1400° C for 2 h under a purified hydrogen atmosphere. The samples were then rolled to the required thickness using several intermediate annealing treatments at 1400° C. After the elaboration treatment, the main impurities were as follows: carbon 21 ppm, nitrogen 13 ppm, oxygen 1000 ppm.

The structural transformations of the different alloys were mainly studied by dilatometric analysis carried out either under purified hydrogen atmosphere using a DHT 60 dilatometer (in this apparatus, the length of the sample is continuously compared with a standard alumina sample; the heating and cooling rates were equal to 300 deg h^{-1}), or an LK 02 dilatometer in order to use higher heating and cooling rates; the tests were then performed under a helium atmosphere). The formation of γ-austenite and ε-martensite was detected by X-ray diffraction.

Electron microscopy examinations were carried out with a JEOL 100C under 100 keV. Thin foils were obtained by anodic dissolution in a Struers apparatus with a double-jet method using 725 cm^3 of methanol, 175 cm^3 of monobutylic ether of glycol ethylene and 100 cm^3 of perchloric acid, under 60 V, with a current density 0.2 A cm^{-2} at $-10°$ C.

0022–2461/85 $03.00 + .12

TABLE I Alloy characteristics

Powder	Origin	Chemical composition (wt %)		Average size of particles (μm)
Fe*	Office National des Industries de l'Azote	Fe	99.8 to 99.9	4 to 5
		C	0.05	
		O_2	0.10	
		N_2	0.10	
Ni*	International Nickel Company	C	0.05 to 0.10	4 to 7
		O_2	0.10	
		Fe	0.01	
		S	0.001	
Co†	Ugine Carbone	Co	99.8	1.5 to 1.9
		Ni	0.04	
		Fe	0.04	
		SiO_2	0.03	
		CaO	0.06	
Mn	Koch-Light Laboratories	Mn	99.95	1 to 15
		Cu	0.01	
		Fe	0.01	
		Si	0.01	

*Ex-carbonyl
†Reduction of CoO_3 by H_2

3. Structural evolution occuring during anisothermal cycles performed at different rates

3.1. Experimental results

3.1.1. 78Fe–12Mn alloy

At the end of the elaboration, at room temperature, the alloy 78Fe–12Mn is two-phased, containing α' and ε-martensites. The ε phase is less important than α'.

During the course of the first dilatometric cycle, performed between 20 and 1000° C, at the heating rate of 300 deg h^{-1} (Fig. 1), one can observe first (Curve 0) a normal thermal expansion up to 300° C; secondly beyond this temperature and up to 370° C, a poor dilatation corresponding to the $\varepsilon \rightarrow \gamma$ transformation. The $\alpha' \rightarrow \gamma$ structural transformation which occurs with a contraction starts only around 500° C. It is difficult to define a precise A_{s0} point (which corresponds to the beginning of the $\alpha' \rightarrow \gamma$ transformation), due to the continuous curvature of the dilatometric curve in the 400 to 550° C temperature range. An accurate acceleration of the $\alpha' \rightarrow \gamma$ transformation can be noted between 660 and 690° C corresponding to the A_{f0} point (i.e. the end of the $\alpha \rightarrow \gamma$ transformation).

During the cooling of the sample from 1000° C (Curve 0′) only an important expansion associated with the $\gamma \rightarrow \alpha'$ transformation starting at 225° C can be observed. This corresponds to the M_{s0} point (i.e. the beginning of the martensitic transformation). After a second heating performed on the same sample, the $\varepsilon \rightarrow \gamma$ transformation is still observed. One can deduce that the reverse $\gamma \rightarrow \varepsilon$ transformation was very likely to occur during the first cooling, but the dimensional change was hidden by the strong expansion corresponding to the $\gamma \rightarrow \alpha'$ transformation. The important expansion observed from 225° C during the first cooling (Curve 0′) can therefore be explained as the result of two simultaneous transformations to which are associated two dimensional variations of opposite direction: (a) a strong expansion due to the main $\gamma \rightarrow \alpha'$ transformation, and (b) a small contraction due to the $\gamma \rightarrow \varepsilon$ transformation.

3.1.2. Influence of molybdenum addition on the structural transformations of the Fe–12Mn alloy

After elaboration treatment, the Fe–12Mn–5Mo alloy consists mainly of α'-lath martensite. However, a small amount of ε-martensite is present in the alloy. The molybdenum addition to the Fe–12Mn binary alloy leads to the following observations (Fig. 1a): (a) the expansion beginning from 290° C associated with the $\varepsilon \rightarrow \gamma$

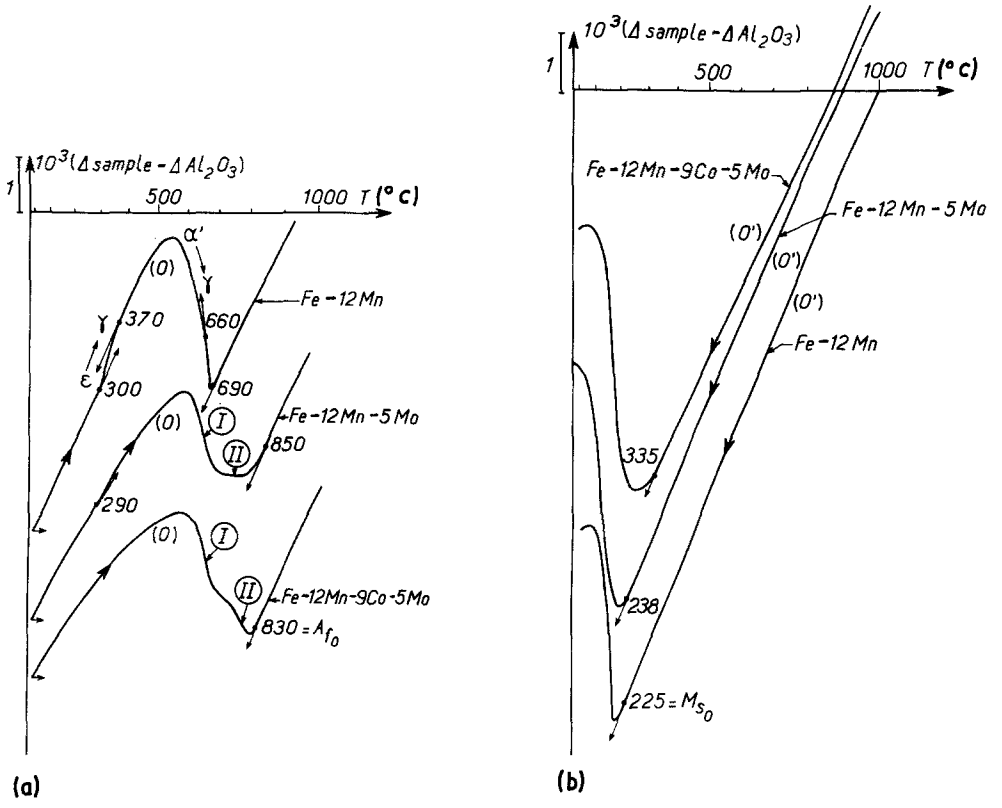

Figure 1 Dilatometric curves recorded at a rate of 300 deg h^{-1} under an atmosphere of hydrogen for the Fe–12Mn alloy containing molybdenum and (Co + Mo) addition: (a) heating, (b) cooling.

transformation now only exhibits a very small amplitude (Curve 0), and (b) the $\alpha' \rightarrow \gamma$ transformation takes place in two successive stages: (a) the first one is a strong contraction, and (b) the second one is equally a contraction but with a small amplitude. This behaviour is quite similar to the one observed with Fe–18Ni–5Mo alloy [18].

During the course of the cooling (Fig. 1b, Curve 0'), we can only observe the important expansion associated with the resultant of the two different transformations $\gamma \rightarrow \alpha'$ and $\gamma \rightarrow \varepsilon$. It may be noted that the M_{s0} point of this ternary alloy is slightly higher (238° C) than the one observed on Fe–12Mn binary alloy (225° C).

3.1.3. Influence of manganese addition on the structural transformations of the Fe–5Mo binary alloy

Fig. 2 represents the heating and cooling curves recorded by dilatometric measurements on different ternary alloys. For all the alloys, the molybdenum content is identical and equal to 5 wt %, whereas the manganese content ranges from 10 to 14 wt %. After the elaboration treatment, these ternary alloys consist only of α'-lath martensite (Fe–10Mn–5Mo) or mainly of α' martensite (Fe–12Mn–5Mo, Fe–13Mn–5Mo) associated with a very small quantity of ε martensite and with austenite whose quantity increases with increasing manganese content up to 14 wt %.

During a first heating (Curves 0) of these different alloys (a) the $\varepsilon \rightarrow \gamma$ transformations is either not observed or observed only very weakly around 290° C; and (b) the $\alpha' \rightarrow \gamma$ transformation takes place in two quite distinct stages: the first (Stage I) exhibits an important contraction, while the second (Stage II) shows a contraction with a small amplitude compared to the one associated with the Stage I.

As in the case of the Fe–12Mn alloy, the precise determination of the A_{s0} point is difficult due to the curvature of the dilatometric curve preceding the $\alpha' \rightarrow \gamma$ transformation, as mentioned above. However, a rough decrease of the A_{s0} and A_{f0} temperatures can be noted as a function of the increasing content of added manganese.

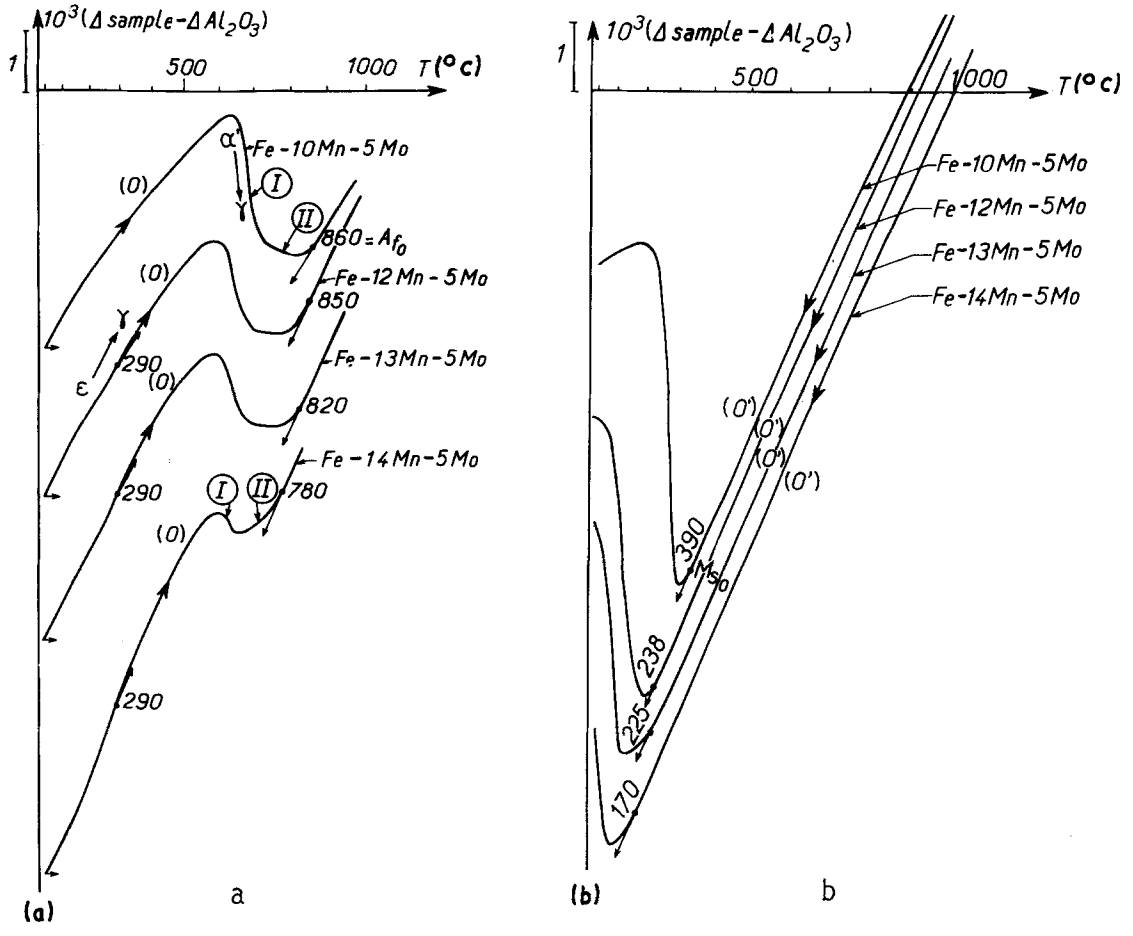

Figure 2 Dilatometric curves recorded at a rate of 300 deg h^{-1} under an atmosphere of hydrogen for the Fe–5Mo alloy containing an addition of manganese increasing up to 14 wt % (a) heating, (b) cooling.

During the course of the first cooling (Fig. 2b, Curves 0′) only an expansion associated mainly with the $\gamma \rightarrow \alpha'$ transformation can be noted; the M_{s_0} point is decreasing with the increasing manganese content; consequently, the $\gamma \rightarrow \alpha'$ transformation is not finished at room temperature for the Fe–13Mn–5Mo and Fe–14Mn–5Mo alloys.

3.1.4. Influence of cobalt on the structural transformations of the Fe–Mn–Mo alloys

Fig. 3 exhibits, among other things, the dilatometric evolution of the Fe–12Mn–4Co–5Mo alloys. After the elaboration treatment, these quaternary alloys consist only of α'-lath martensite.

It can be observed (Curves 0) that the $\alpha' \rightarrow \gamma$ transformation occurs in two distinct successive stages which are two important contractions, the amplitudes of which are more or less different according to the cobalt content of the alloy: in fact, with a small cobalt content, the amplitude of the first contraction is more important whereas the amplitude of the second one is smaller.

During the cooling (Curves 0′), the $\gamma \rightarrow \alpha'$ transformation only takes place in a single stage associated with an important expansion. The M_{s_0} point increases with the increasing cobalt content of the alloy. These results are quite similar to those observed in the case of the Fe–Ni–Co–Mo quarternary alloys [18]. The Fe–18Mn–9Co–5Mo consists only of ε-martensite and it may be noted that the $\varepsilon \rightarrow \gamma$ and $\gamma \rightarrow \varepsilon$ transformations show a certain hysteresis.

3.2. Interpretation of the results

In order to compare our present results, as far as

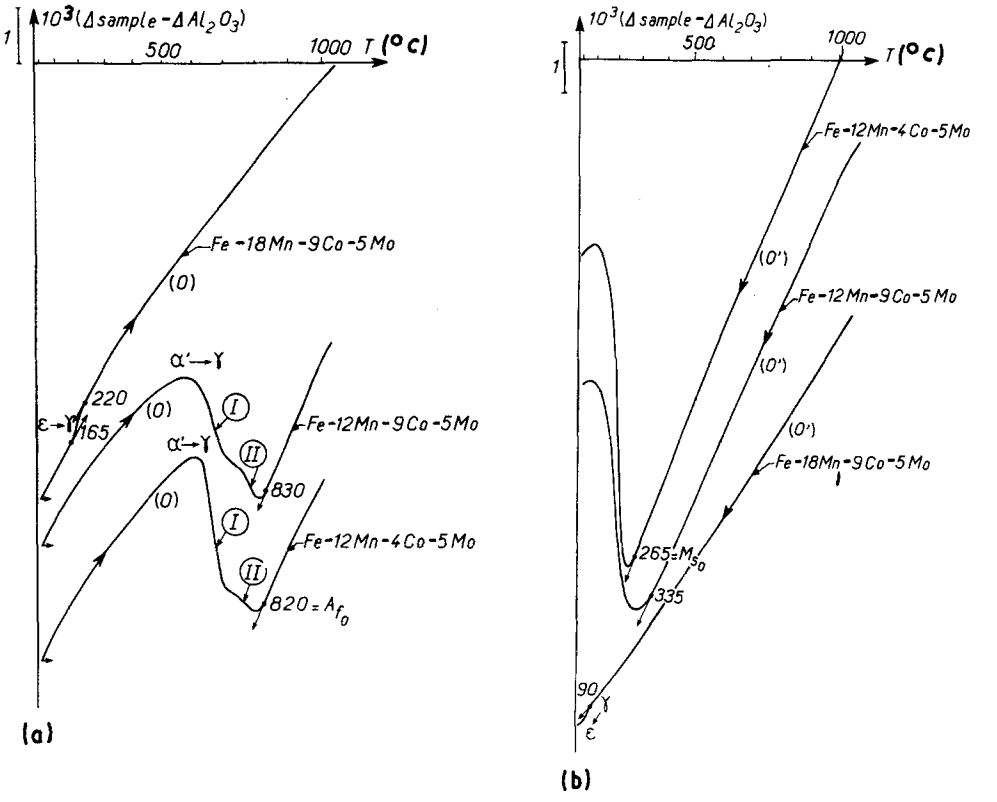

Figure 3 Dilatometric curves recorded at a rate of 300 deg h^{-1} under an atmosphere of hydrogen for Fe–Mn–Co–Mn quaternary alloys: (a) heating, (b) cooling.

the mechanisms of the austenitic transformation are concerned, with those previously obtained on the ternary alloy 74.1Fe–20.4Ni–5.3Mo and on the quaternary alloys 67.4Fe–18.6Ni–8.9Co–4.8Mo, of maraging type, three alloys with the following wt % were studied: 83Fe–12Mn–5Mo; 82Fe–13Mn–5Mo; and 74Fe–12Mn–9Co–5Mo.

3.2.1. 83Fe–12Mn–5Mo alloy

During cooling succeeding to an interrupted heating, (a) in the first stage of the $\alpha' \rightarrow \gamma$ transformation (Fig. 4) no M_s point is observed: the austenite formed is stable down to room temperature (Curve 1′); and (b) in the second stage, a martensitic transformation takes place, and develops in either two or one stages.

In a two-stage transformation the first stage, beginning at 248° C, corresponds to the $\gamma \rightarrow \alpha'$ transformation. Beyond 178° C (Curve 2′), the lowering of the expansion corresponds to the beginning of the $\gamma \rightarrow \varepsilon$ transformation, while the $\gamma \rightarrow \alpha'$ transformation simultaneously continues. A subsequent heating (Curve 2″, Fig. 5) from 210° C shows a slight expansion associated with the $\varepsilon \rightarrow \gamma$ transformation. It can therefore be noted that the temperature of the beginning of the $\gamma \rightarrow \varepsilon$ or $\varepsilon \rightarrow \gamma$ transformations seem to be dependent upon either the temperature reached in the austenitic transformation range or the lowest temperatures of the γ field (as in the case of the $\alpha' \rightarrow \gamma$ or $\gamma \rightarrow \alpha'$ (transformations).

In a single-stage transformation (Curve 3′, Fig. 4) the M_s points of the $\gamma \rightarrow \alpha'$ transformations are always higher (248 and 320° C) than the M_{s_0} point (238° C).

3.2.2. 82Fe–13Mn–5Mo alloy

During the cooling succeeding an interrupted heating in Stage II of the martensitic transformation (Curve 1′, Fig. 6), the two $\gamma \rightarrow \alpha'$ and $\gamma \rightarrow \varepsilon$ martensite transformations are clearly observed. They exhibit dimensional changes of opposite sign. The reheating cycle (Curve 1″, Fig. 6) compared to Curve 1′ shows well the hysteresis which exists between the $\gamma \rightarrow \varepsilon$ and $\varepsilon \rightarrow \gamma$ temperature transformations, as well as the difference between the amplitudes of the transformations occuring during the cooling and

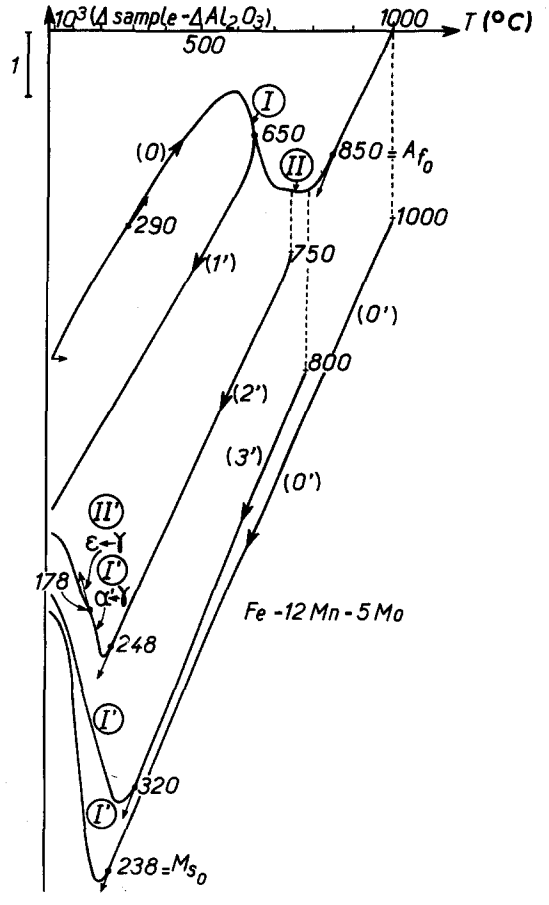

Figure 4 Dilatometric curves recorded at a rate of 300 deg h^{-1} under an atmosphere of hydrogen during cooling interrupted at different temperatures in the $\alpha \rightarrow \gamma$ transformation range for the Fe–12Mn–5Mo alloy.

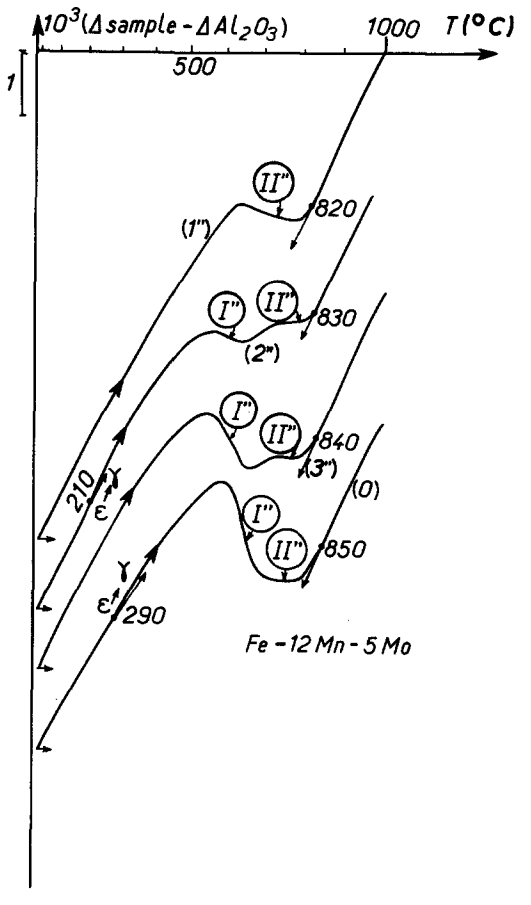

Figure 5 Dilatometric curves recorded during reheatings subsequent to the coolings represented in Fig. 4.

the heating; such a phenomenon was previously observed by Tolba [19] in the case of Fe–15Mn and Fe–17.5Mn alloys (wt %). The smaller amplitude of the contraction associated with the $\gamma \rightarrow \varepsilon$ transformation is probably related to an expansion due to the $\gamma \rightarrow \alpha'$ transformation which partially compensates the above $\gamma \rightarrow \varepsilon$ anomaly.

3.2.3. 84Fe–12Mn–9Co–5Mo alloy

In Fig. 7, Curve 1′ shows that the austenite formed in Stage I of the $\alpha' \rightarrow \gamma$ transformation remains stable down to room temperature. When Curves 0′, 1′ → 5′ are compared, it can be seen that the M_s point increases as a function of the temperature reached in Stage II during the prior heating, and this is observed even for temperatures higher than the A_{f_0} point. We already have observed such a phenomenon in the case of the 74.1Fe–20.4Ni–5.3Mo ternary alloy [18] and interpreted it as a consequence of a non-homogeneous austenitic composition just beyond the A_{f_0} point. To carry out homogenization treatment, it is then very important to select a temperature markedly superior to the A_{f_0} point, such as 1000° C.

Taking into account the resemblance of the results observed on nickel and/or manganese based alloys, the authors consider that the interpretation previously proposed [18] to explain the $\alpha' \rightarrow \gamma$ transformation is still valid: for relatively slow (300 deg h^{-1}) heating or cooling rates considered in this part of the paper, we can emphasize that the mechanisms regulating the $\alpha' \rightarrow \gamma$ transformation mainly involve the diffusion of the addition elements. Precipitation occurs during the heating before reaching the A_{s_0} point, as will be further demonstrated. This

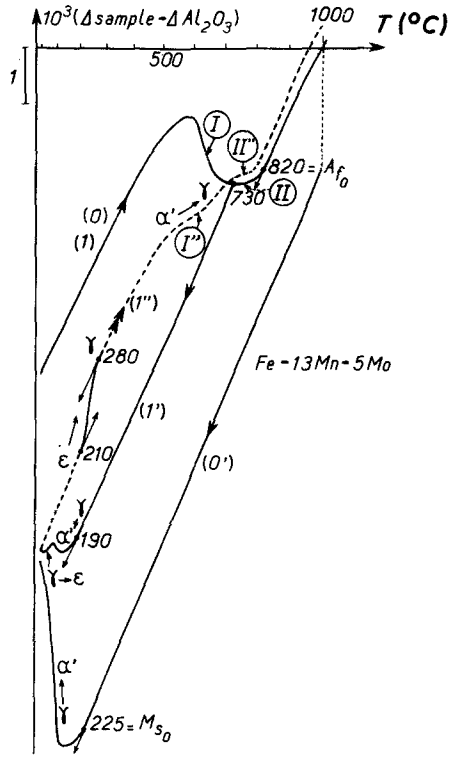

Figure 6 Dilatometric curves recorded at a rate of 300 deg h^{-1} under an atmosphere of hydrogen for the alloy Fe–13Mn–5Mo.

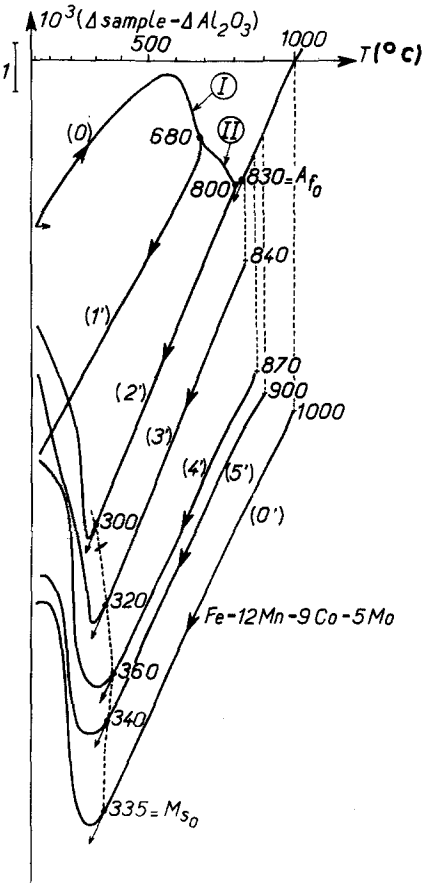

Figure 7 Dilatrometric curves recorded at a rate of 300 deg h^{-1} under an atmosphere of hydrogen for the alloy Fe–12Mn– 9Co–5Mo.

precipitation leads to a heterogeneity in the α' martensite as far as the addition element contents are concerned: i.e. α' zones respectively enriched or depleted in these elements, in particular (Mn + Mo), are referred to as α'_E and α'_D.

The first step (Stage I) of the transformation $\alpha' \rightarrow \gamma$, for which M_s points have been found to be always below M_{s_0}, represents the transformation of the α'_E phase according to the following process:

$$\alpha'_E \rightarrow \alpha_{ED} + \gamma_{EE}$$

The second step (Stage II) of this transformation, having M_{s_0}, represents the transformation of both phases

$$\begin{cases} \alpha_{ED} \rightarrow \alpha_{EDD} + \gamma_{EDE} \\ \alpha'_D \rightarrow \alpha_{DD} + \gamma_{DE} \end{cases}$$

$$\text{with } C_{\gamma DE} < C_0 < C_{\gamma EDE} < C_{\gamma EE}$$

C_0 represents the concentration of the addition elements (Ni + Mo) or (Mn + Mo) of the homogeneous α' martensite.

3.2.4. *Influence of heating and cooling rates on the austenitic and martensitic transformations*

One can observe, as a function of the heating rate, increasing from 0.08° sec^{-1} to 50 deg sec^{-1}, that the austenitic transformation starts at a temperature which is higher than the one determined for usual heating rates in the apparatus used, i.e. 300° h^{-1} = 0.08 deg sec^{-1} (see Table II relative to the Fe–12Mn–9Co–5Mo alloy).

TABLE II Transformations in Fe–12Mn–9Co–5Mo alloy

Heating rate (deg sec^{-1})	A_{s_0}	A_{f_0}	M_{s_0}
0.08	~550	830	335
1	670	910	340
5	700	920	340
50	735	920	340

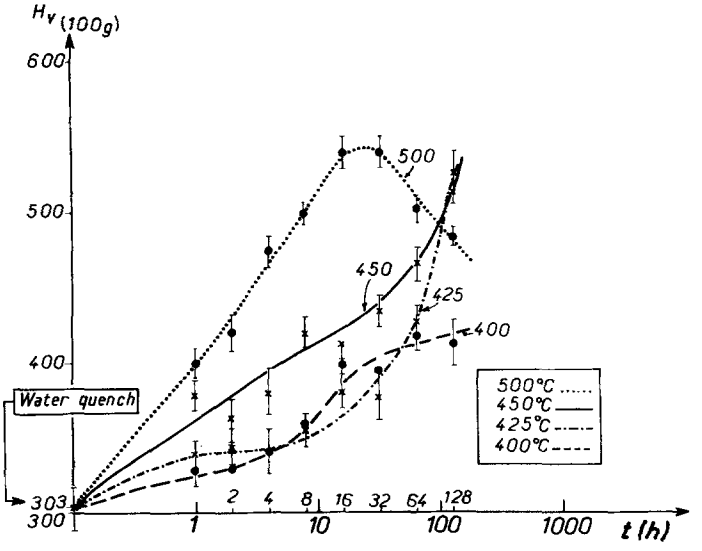

Figure 8 Vickers microhardness measurements as a function of time for different ageing temperatures in the case of the Fe–12Mn–9Co–5Mo alloy.

Stage I always exhibits an important contraction, whereas Stage II is only revealed by a slight change of the slope, which tends to disappear while the heating rate increases. When the heating rate becomes higher than about 20 deg sec^{-1}, the austenitic transformation only takes place in a single stage; under such conditions, the transformation mechanism mainly involves a shear process.

An expansion with an important amplitude is always associated with the martensitic transformation, whereas the M_s point does not change in practice. It can therefore be concluded, as for the Fe–Ni–Mo and Fe–Ni–Co–Mo alloys, that an increase in the heating rate tends to diminish the diffusional phenomena which take place before or during the austenitic transformation.

4. Precipitation phenomena occurring before the A_{s_0} point in martensite

In what follows only the case of the Fe–12Mn–9-Co–5Mo will be considered.

4.1. Vickers microhardness

Vickers microhardness measurements (H_V 1N) show that two precipitation stages can be determined for low ageing temperatures of 400 to 425° C (Fig. 8). The first stage is characterized by a small increase in the microhardness (about 50 points) and seems to be longer when the temperature is low, whereas an important increase in the microhardness is associated with the second stage. As above, this stage is longer for lower temperatures. In the case of the highest ageing temperature considered in this paper (500° C), after 16 h a decrease in the microhardness is observed which corresponds both to the formation of reversed austenite (detected by electron microscopy on thin foils) and over-ageing phenomena.

4.2. Electron microscopy and microdiffraction

4.2.1. Elaboration microstructures

After the elaboration treatment the Fe–12Mn–9Co–5Mo alloy, examined at 20° C, shows a lath martensite type structure with a high density of dislocations (Fig. 9). No trace of ε-martensite was detected.

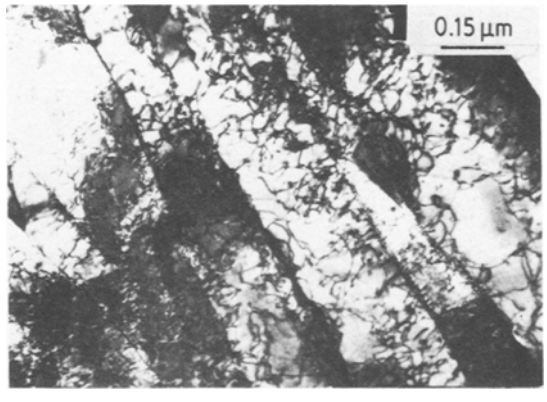

Figure 9 Bright-field micrograph of the Fe–12Mn 9Co–5Mo alloy after the elaboration treatment.

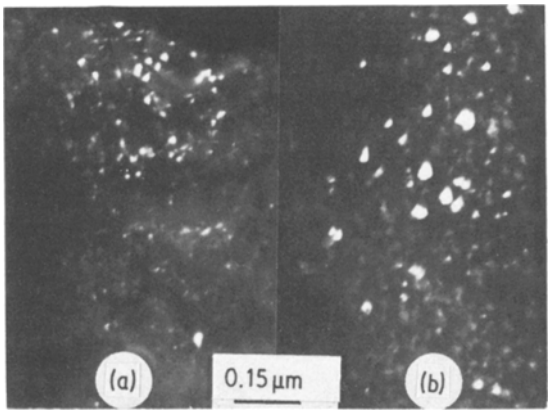

Figure 10 Dark-field micrograph showing the Fe_2Mo precipitates observed in the Fe–12Mn–9Co–5Mo alloy aged at 400° C during (a) 32 h; (b) 100 h.

4.2.2. Ageing microstructures

In thin foils, aged in the first ageing stage defined by microhardness measurements, no precipitates were found; whereas in the second stage, precipitates of isothermal ω phase and Fe_2Mo were observed. Their size and relative fraction depend upon the temperature and the ageing time.

For lower temperatures, such as 425° C after 32 h, one can first observe (and only here and there) small spherical precipitates of Fe_2Mo with an average diameter of 10 nm (Fig. 10a). The Fe_2Mo intermetallic compound has a hexagonal structure with the following parameters: $a = 0.473$ nm, $c = 0.772$ nm, i.e. $c/a = 1.632$. When the ageing time increases (i.e. 100 h at this same temperature), the precipitates of Fe_2Mo grow significantly (Fig. 10b).

At higher temperatures (i.e. at 450° C for 128 h) large precipitates of Fe_2Mo, with also a globular shape of about 50 nm diameter (Fig. 11a) and ω phase precipitates (Fig. 13a below) with a form and a size similar to that of Fe_2Mo are simultaneously observed. The diffraction pattern with the $\langle 1\,1\,0 \rangle$ martensite zone axis corresponding to only the Fe_2Mo phase is represented in Fig. 11b. The key (Fig. 11c) shows the different diffraction spots corresponding to four families designated F_1 to F_4 and are the most frequently observed as a function of the intensity of their diffraction spots.

Fig. 12 relates to ω phase precipitates formed after an ageing performed at 420° C for 48 h in the case of the 67.4Fe–186.Ni–8.9Co–4.8Mo. These precipitates exhibit an average diameter of about ~ 5 nm. The ω phase of this alloy was previously described as having a hexagonal structure with the parameters $a = 0.390$ nm, $c = 0.248$ nm and $c/a = 0.636$ [20].

Theoretically, no diffraction spot given by the ω phase should be observed on the $\langle 0\,0\,1 \rangle_M$ zone axis [21]. In fact, diffraction spots with a weak intensity are observed at 1/3 and 2/3 of the

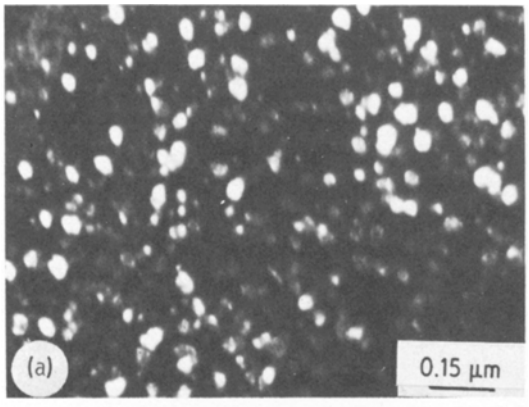

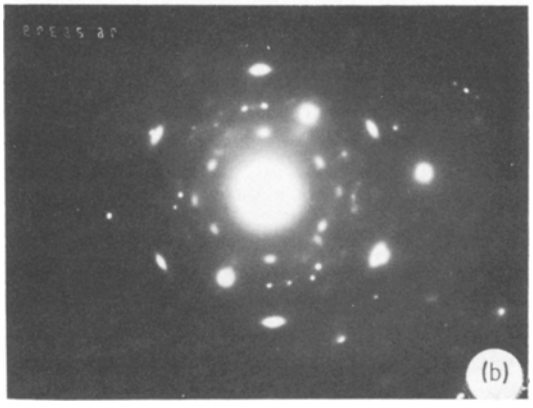

Figure 11 (a) Dark-field micrograph showing the Fe_2Mo precipitates observed in the Fe–12Mn 9Co–5Mo alloy aged at 450° C for 128 h. (b) $\langle 1\,1\,0 \rangle_M$ zone axis diffraction pattern; (c) key to (b) showing four families of Fe_2Mo precipitates.

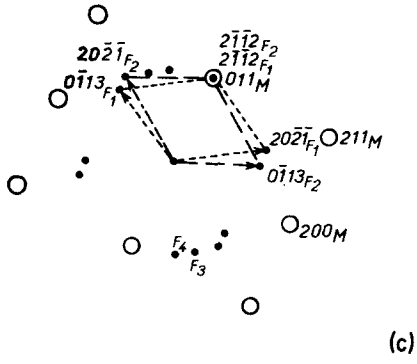

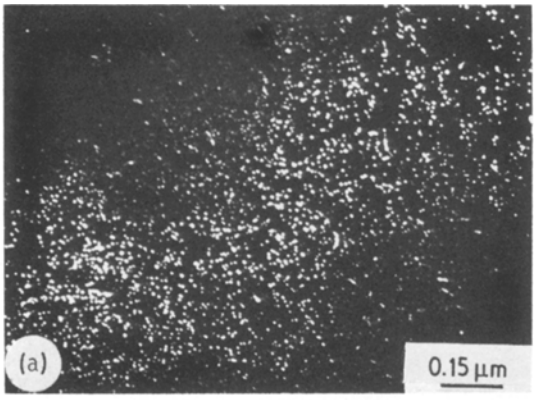

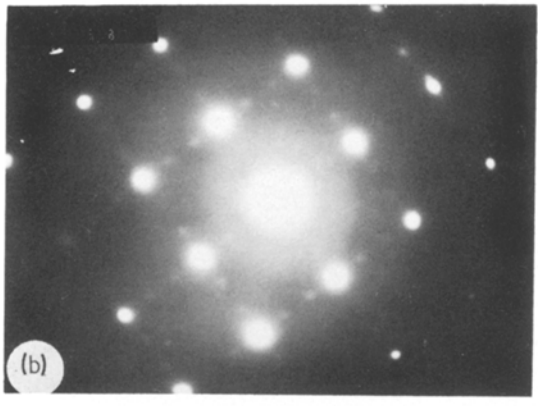

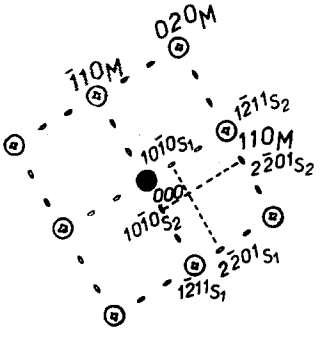

(c)

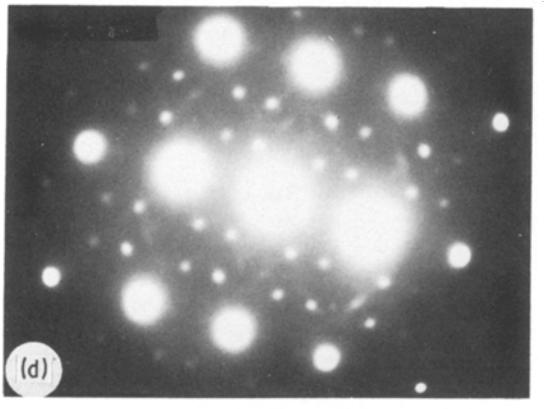

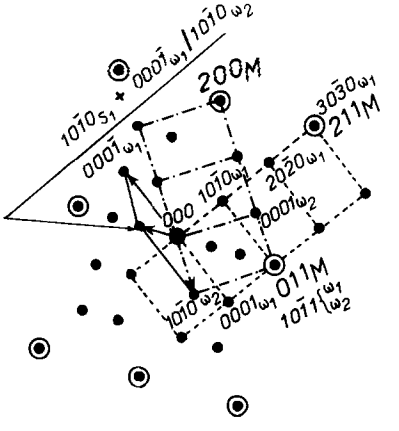

(e)

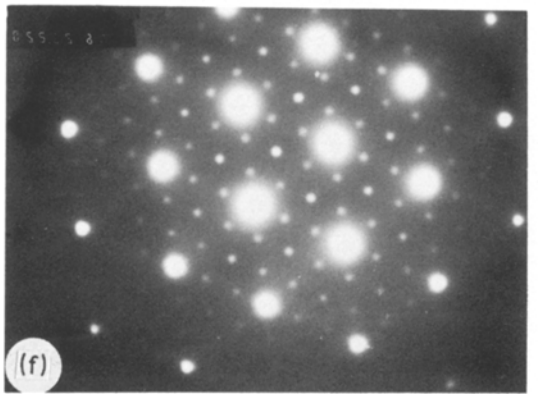

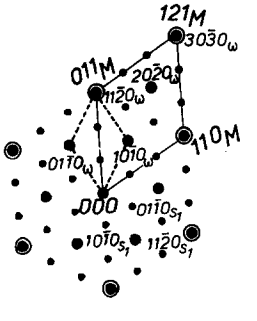

(g)

Figure 12 (a) Dark-field micrograph showing the ω phase precipitates observed in the Fe-18, 5Ni–8, 9Co-4, 8Mo aged at 420° C during 48 hours. (b) $\langle 0\,0\,1\rangle_M$ zone axis diffraction pattern; (c) key to (b). (d) $\langle 1\,1\,0\rangle_M$ zone axis diffraction pattern; (e) key to (d). (f) $\langle 1\,1\,1\rangle_M$ zone axis diffraction pattern; (g) key to (f).

$\langle 1\,1\,0\rangle_M^*$ directions (Fig. 12b) [20, 22, 23]. Yedneral and Perkas [20] have interpreted these diffraction spots as being due to a superlattice, called S in the following, with a hexagonal structure and parameters $a = 0.704$ nm and $c = 0.248$ nm, i.e. $c/a = 0.352$, whose formation precedes that of the ω phase. These authors proposed in fact a continuous evolution of this S phase from A_8B, through A_7B_2 until A_6B_3. The chemical composition of ω phase can be written as A_2B with A = Fe, Ni, Co and B = Mo; while its crystallography can be described as a hexagonal structure with $a = 0.390$ nm and $c = 0.248$ nm.

In the case of the Fe–Mn–Co–Mo quaternary alloy, under consideration in this paper, extra diffraction spots were observed on the $\langle 0\,0\,1\rangle_M$ zone axis pattern of the ω phase (Fig. 13b). Furthermore, extra spots appearing at 1/3 and 2/3 of the $\langle 2\,0\,0\rangle_M^*$ directions are also obtained; these latter were interpreted as resulting from double diffraction phenomena occuring between the $\{1\,0\,\bar{1}\,0\}$ diffraction spots of the two S_1 and S_2 families of precipitates having the S structure of the superlattice (Fig. 13c).

Fig. 12d shows the $\langle 1\,1\,0\rangle_M$ zone axis diffraction pattern. The ω phase spots are given by two families of the ω phase of the Fe–Ni–Co–Mo alloy. The key is given by Fig. 12e. It should be noted that the diffraction spots appearing at 1/3 and 2/3 of the $\langle 1\,1\,0\rangle_M^*$ direction are still observed as in Fig. 12b. For the Fe–Mn–Co–Mo alloy, the $\langle 1\,1\,0\rangle_M$ zone axis diffraction pattern is more complex: one can observe simultaneously the diffraction spots of two families of ω phase precipitates and those of four families of Fe_2Mo precipitates (see Figs. 11b and c).

Fig. 12f relates to the Fe–Ni–Co–Mo alloy and corresponds to the $\langle 1\,1\,1\rangle_M$ zone axis diffraction pattern, which is the only one to show that the ω phase of this alloy has an ordered structure, as revealed by the extra diffraction spots of the $\{1\,0\,\bar{1}\,0\}$, $\{2\,0\,\bar{2}\,0\}$ type, which are forbidden due to their structure factor in the case of the disordered ω phase [20]. In fact, the observation of these spots (referred as $\{1\,0\,\bar{1}\,0\}_{\omega_1}$ and $\{1\,0\,\bar{1}\,0\}_{\omega_2}$ on the $\langle 1\,1\,0\rangle_M$ zone axis diffraction pattern) could either signify that the ω phase from which they issue is ordered, or that these spots are due to a double diffraction phenomena between the $\{1\,1\,0\}_M$ and $\{0\,0.1\}_\omega$ diffraction spots. In Fig. 12f, showing the $\langle 1\,1\,1\rangle_M$ zone axis diffraction, the occurrence of the $\{1\,0\,\bar{1}\,0\}_\omega$ and $\{2\,0\,\bar{2}\,0\}_\omega$ and $\{2\,0\,\bar{2}\,0\}_\omega$ diffraction spots cannot be due to a double diffraction phenomena; in consequence, the ω phase is ordered in the Fe–Ni–Co–Mo alloys.

The diffraction pattern represented in Fig. 13f shows, in the case of the Fe–Mn–Co–Mo alloy, that the ω phase is also ordered. Furthermore, the diffraction spots arising from different families of Fe_2Mo precipitates should also be noted on this pattern; only two families are indicated on Fig. 13g and they are referred as F_1 and F_2. These two types of small precipitates (ω and Fe_2Mo) give rise to the hardening phenomena observed during ageing. However, in the case of the nickel maraging steel the size of the ω phase precipitates, which remain always very small (diameter about ~ 5 nm) confer on this alloy a more important hardening than the one occurring in the manganese maraging type alloy.

In the case of the nickel maraging steel, on the $\langle 1\,1\,0\rangle_M$ zone axis diffraction pattern it will also be noted that the ω phase diffraction spots are almost aligned along the $\langle 1\,1\,2\rangle_M^*$ directions (Fig. 12d); whereas in the case of the manganese maraging steel, these same diffraction spots are clearly displaced from one part to another of this same $\langle 1\,1\,2\rangle_M^*$ direction. Similar observations were made on diffraction patterns given by the ω phase of titanium alloys, and were related to the content in some elements of this phase [24].

The precipitates of Fe_2Mo are semi-coherent with the martensitic matrix. The orientation relationships previously determined [25] are the following:

$$\{2\,\bar{1}\,\bar{1}\,2\}_{Fe_2Mo} \| \{1\,1\,0\}_{\alpha'}$$
$$\text{and} \quad \langle \bar{2}\,4\,3\rangle_{Fe_2Mo} \| \langle 1\,1\,1\rangle_{\alpha'} \qquad (1)$$

This relation theoretically gives rise to the observation of 24 families of precipitates. On some diffraction patterns, we could only distinguish clearly a maximum of eight different families of precipitates. It will be noted, from the diffraction pattern shown in Fig. 11b, that the orientation relationship between the Fe_2Mo precipitates and the martensitic matrix is the following:

$$\{2\,\bar{1}\,\bar{1}\,2\}_{Fe_2Mo} \| \{1\,1\,0\}_{\alpha'}$$
$$\text{and} \quad \langle 1\,6\,2\rangle_{Fe_2Mo} \| \langle 1\,1\,1\rangle_{\alpha'} \qquad (2)$$

For higher ageing temperatures under consideration in this work (500° C), the simultaneous

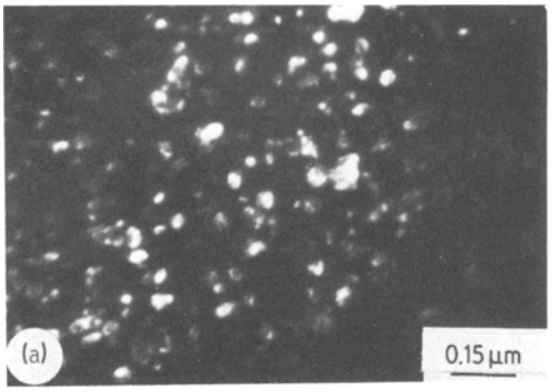

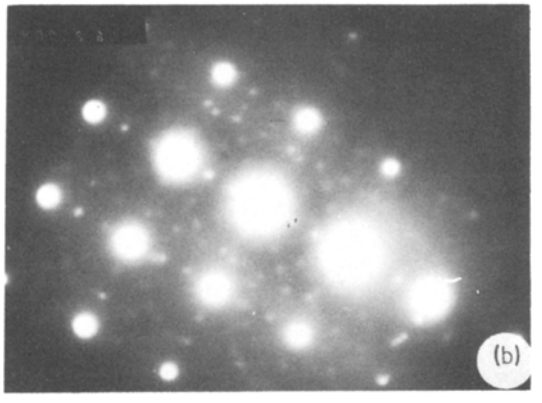

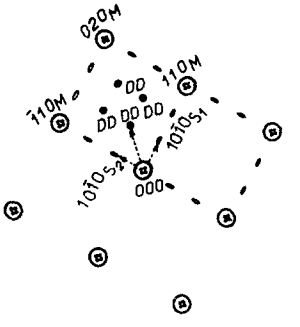

(c)

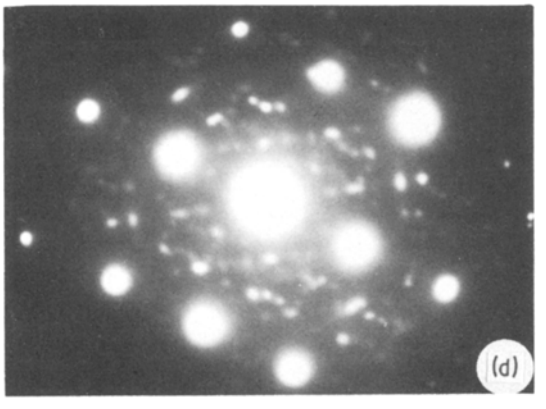

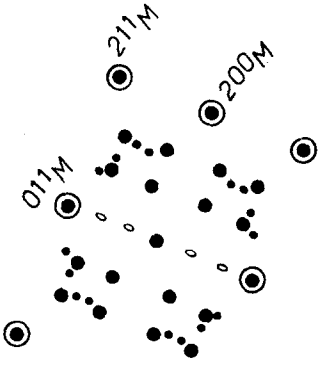

(e)

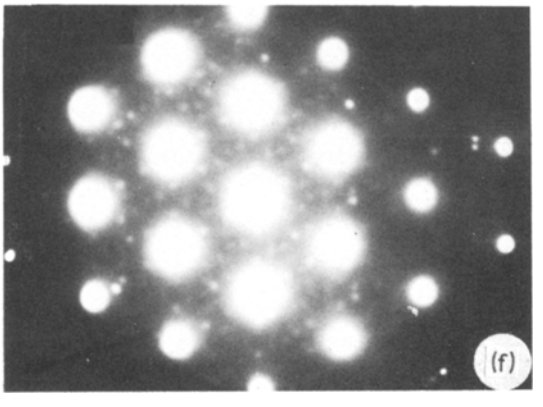

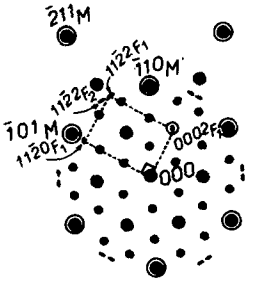

(g)

Figure 13 (a) Dark-field micrograph showing the ω phase precipitates observed in the Fe–12Mn–9Co–5Mo alloy aged at 450° C for 128 h. (b) $\langle 0\,0\,1 \rangle_M$ zone axis diffraction pattern; (c) key to (b). (d) $\langle 1\,1\,0 \rangle_M$ zone axis diffraction pattern; (e) key to (d). (f) $\langle 1\,1\,1 \rangle_M$ zone axis diffraction pattern; (g) key to (f).

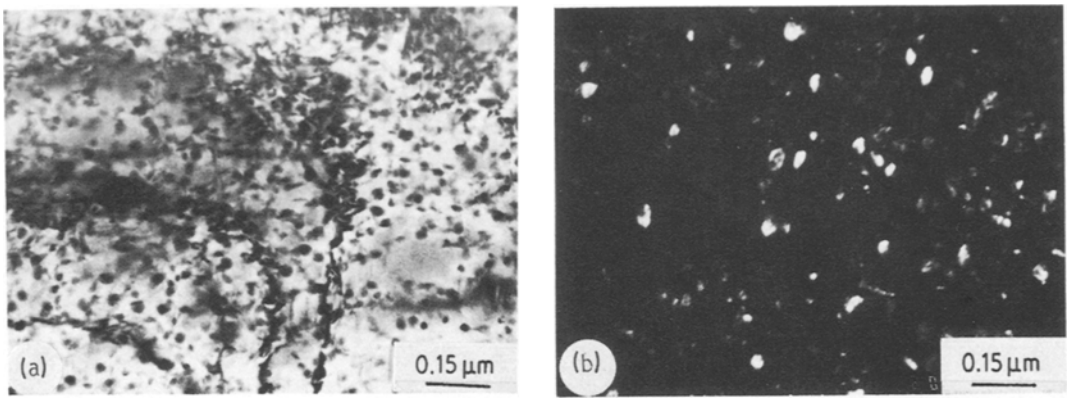

Figure 14 (a) Bright-field micrograph observed on the Fe–12Mn–9Co–5Mo alloy aged at 500° C for 4 h. (b) Dark-field micrograph obtained from an ω phase diffraction spot observed on the Fe–12Mn–9Co–5Mo alloy aged at 500° C for 16 h.

occurrence of the ω and Fe_2Mo phase formation will be noted (Fig. 14). After 16 h of ageing time, small patches of reversed austenite begin to be observed.

5. Conclusions

It can be concluded from this work that in the case of either Fe–Mn–Mo ternary of Fe–Mn-Co–Mo quaternary manganese maraging alloy, the structural evolution taking place during anisothermal or isothermal treatments performed is similar to that of the Fe–Ni–Mo and/or Fe–Mi–Co–Mo alloys. The dilatometric analysis of these manganese alloys, the microstructure of which consists of either only b.c.c. α'-martensite, or of α'-martensite with a very small amount of ε-martensite with a hexagonal structure, showed that:

(a) The α'-martensite $\rightarrow$ austenite transformation takes place in a single or several successive stages according to the manganese, cobalt and molybedenum content for heating rates of about 300 deg h^{-1}. An important contraction is always associated with the first stage, whereas the second stage exhibits either a slight change of slope of the dilatometric curve, or a contraction with a more or less strong amplitude depending upon the manganese, cobalt and molybdenum.

(b) The martensite $\rightarrow$ austenite transformation changes as a function of the heating rate, varying from 0.08 deg sec^{-1} (300 deg h^{-1}) to 50 deg sec^{-1}. In fact, even if, in the case of an 0.08 deg sec^{-1} heating rate, the alloy exhibits a martensite $\rightarrow$ austenite transformation occuring in two successive and clearly distinct stages for rapid heating rates, the $\alpha' \rightarrow \gamma$ transformation occurs in a single step.

(c) Different heatings interrupted in the single or the several stages associated with the $\alpha' \rightarrow \gamma$ transformation provoke a very clear evolution of the M_s points during subsequent coolings; these observations suggest the occurence of diffusional phenomena during this transformation.

(d) The $\gamma \rightarrow \alpha'$ martensite transformation takes place in a single step and exhibits a strong expansion in the case of the alloy homogenized at temperatures higher than A_{f_0}. We have again observed that molybdenum addition lowers the M_s point, while cobalt addition increases it as in the case of the Fe–Ni–Co–Mo alloys.

Furthermore, precipitation phenomena occur into the α' martensite before the A_{s_0} point. The precipitates were studied, under isothermal conditions, by microhardness measurements and electron microscopy on thin foils. This study has shown that:

(a) The ageing occurs in a single or two successive stages depending upon the ageing temperature which varies from 400 to 500° C.

(b) The hardness values obtained for the same temperatures and ageing times are less important than in the case of nickel maraging steels. In the case of manganese alloys, the larger size of the precipitates could partly explain these results.

(c) Depending upon the ageing temperature and time, the Fe_2Mo intermetallic compound with a hexagonal structure, and an isothermal ω phase with an ordered hexagonal structure are present in the α' martensite either simultaneously or separately.

References

1. R. F. DECKER, R. B. G. YEO, J. T. EASH and C. G. BIEBER, *Mater. Design Engng.* **55** (1962) 106.
2. R. F. DECKER, J. T. EASH and A. J. GOLDMAN, *Trans. AMS* **55** (1962) 58.
3. G. MAEDER, Thèse de Doctorat ès-Sciences Physiques, Université de Paris-Sud (1975).
4. J. P. THEVENIN. Thèse de Doctorat de Illème cycle, Université de Paris-Sud (1966).
5. A. GOLDBERG and J. WELD, *Trans. AMS Quart.* **47** (5) (1968) 199.
6. A. GOLDBERG, *ibid.* **61** (1) (1968) 26.
7. G. A. BERESNEV and V. G. GROVALD, *Metal. I. Term. Obra. Metal* No. 6, (June 1968) p. 15.
8. L. N. BELYAKOV, V. L. NIKOL'SKAYA, and S. S. RYZHAK, *ibid.* p. 26.
9. R. BORRELLY, Thèse de Doctorat ès-Sciences Appliquées, Université de Lyon (1965).
10. C. SERVANT, Thèse de Doctorat ès-Sciences Physiques, Université de Paris-Sud (1972).
11. L. PRIESTER, Thèse de Doctorat ès-Sciences Physiques, Université de Paris-Sud (1972).
12. E. JOLLES, Thèse de Doctorat ès-Sciences Physiques, Université de Paris-Sud (1972).
13. R. COURRIER, Thèse de Doctorat ès-Sciences Physiques, Université de Nancy (1972)
14. I. YODOGAWA and S. TANAKA, *Trans. Iron Steel Inst. Jpn* **18** (1978).
15. E. A. BRANDES and R. F. FLINT, "Manganese phase diagrams", edited by Manganese Center, Neuilly sur Seine, France (1980) p. 152.
16. J. MANENC, *Mém. Sci. Rev. Met.* **68** (1971) 761.
17. A. J. BAKER and B. L. GABBITAS, Proceedings of Electron Microscope Conference Canberra, 1974 (Australian Academy of Sciences) p. 670.
18. C. SERVANT and P. LACOMBE, *J. Mater. Sci.* **12** (1977) 1807.
19. S. TOLBA, Thèse de Doctorat d'Ingénieur, Université de Paris-Sud (1981).
20. A. F. YEDNERAL and M. D. PERKAS, *Fis. Metal. Metalloved,* **33** (2) (1972) 315.
21. O. LYON, Thèse de Doctorat ès-Sciences Physiques, Université de Paris-Sud (1982).
22. J. L. SASS, *Acta Metall,* **17** (1969) 813.
23. J. BOURGEOT, P. MAIREPIERRE, J. MANENC and B. THOMAS, Proceedings of 5th International Materials Symposium, Berkeley, California, 1971.
24. J. P. MORNIROLI, Thèse de Doctorat ès-Sciences Physiques, Université de Nancy (1974) p. 80.
25. V. I. KIRIYENKO and L. P. POTAPOV, *Fiz. Metal. Metalloved* **38** (1974) 317.

Received 10 October
and accepted 6 November 1984